Reaction Chemistry & Engineering

ROYAL SOCIETY OF CHEMISTRY

PAPER

View Article Online
View Journal

Cite this: DOI: 10.1039/d5re00332f

Continuous and sensitive monitoring of LPMO reactions using an optical H_2O_2 sensor

Leonor Vieira Carneiro, [ab] Anders Ørts Tjell,[c] María Dolores Fernández-Ramos, [d] Torsten Mayr *[c] and Daniel Kracher *[ab]

Received 29th July 2025,
Accepted 2nd December 2025

DOI: 10.1039/d5re00332f

rsc.li/reaction-engineering

We demonstrate the use of an optical sensor to follow the activity of H_2O_2-dependent enzymes in real-time, using *quasi*-continuous detection of H_2O_2. The sensor enables kinetic measurements of the H_2O_2-consuming enzyme lytic polysaccharide monooxygenase (LPMO) under homogeneous conditions at 1 mL scale conversion assays. By tracking H_2O_2 concentration changes over time during 2-minute reaction intervals, we established quantitative assays and determined Michaelis–Menten kinetics for the LPMO from *Lentinus similis* to cellotetraose, with a K_M value of 0.22 ± 0.08 mM and a maximum reaction rate (V_{max}) of 0.97 ± 0.64 μM s^{-1}. This method allows for continuous monitoring without reliance on time-consuming, discontinuous assays or post-reaction sample processing. We evaluate the capabilities of the sensor to monitor enzyme activity, benchmark it against established spectrophotometric methods, and discuss its limitations and advantages. This work provides a method for the real-time assessment of LPMO kinetics but also enables broader application to other redox enzymes that consume or release H_2O_2 during the reaction.

1 Introduction

Redox enzymes such as peroxidases, peroxygenases and oxidases catalyse a wide range of oxidation and oxyfunctionalisation reactions using hydrogen peroxide (H_2O_2) or molecular oxygen (O_2) as co-substrates.[1–5] Among those, lytic polysaccharide monooxygenases are ubiquitous copper-dependent enzymes[6] that employ a H_2O_2-dependent redox mechanism to cleave recalcitrant polysaccharides such as cellulose and chitin.[7] LPMOs break β-1,4-glycosidic linkages in the substrate through oxidation at the C1 and/or C4 carbons, thereby enhancing the overall efficiency of cellulolytic enzymes.[8–10] As a result, these enzymes can boost commercial cellulase mixtures in biorefinery settings.[11]

LPMOs have been identified in a wide range of host organisms, including bacteria, fungi, plants and insects.[12–14] Based on their substrate scope and sequence, they are classified into multiple auxiliary activity (AA) families in the CAZy database (AA9-11, AA13-15, and AA16-17; http://www.cazy.org). Originally thought to use O_2 as a co-substrate,[6] recent research has demonstrated that LPMOs possess a dominant peroxygenase reactivity that is several orders of magnitude higher than the reaction with molecular oxygen.[7,15–18] While this reaction enables enhanced catalytic efficiency, it also increases the risk of oxidative self-inactivation under substrate-depleted conditions.[7,19–21] The LPMO reaction requires not only externally supplied H_2O_2 but also reduction equivalents, which can be derived from redox partner enzymes or small molecule reductants, such as ascorbic acid.[22]

Activity determination of LPMOs typically relies on chromatographic methods that separate and quantify the diverse soluble oxidised oligosaccharides released from the polysaccharide substrate by LPMOs. This necessitates the availability of oxidised oligosaccharide standards and requires derivatisation or specialised detection techniques such as HPLC-MS/UHPLC-MS, HPAEC-PAD or MALDI-TOF. A detailed overview of chromatographic methods for the qualitative and quantitative analysis of LPMOs is provided elsewhere.[23,24] While indispensable to determine the product profile and gain insight into the mechanistics of the reaction, chromatographic methods are generally not suitable for real-time monitoring of LPMO activity.

Several rapid assays have been developed to monitor LPMO activity using fluorogenic or chromogenic substrates in time-resolved formats.[25] Among these, the Amplex™ Red assay detects the H_2O_2 generated by reduced LPMO through a slow oxygen-dependent uncoupling reaction, but is limited

[a] *Institute of Molecular Biotechnology, Graz University of Technology, Petersgasse 14, 8010 Graz, Austria. E-mail: daniel.kracher@tugraz.at; Tel: +43 316 873 4084*
[b] *BioTechMed-Graz, Graz, Austria*
[c] *Institute of Analytical Chemistry and Food Chemistry, Graz University of Technology, Stremayrgasse 9/II, 8010 Graz, Austria. E-mail: torsten.mayr@tugraz.at; Tel: +43 316 873 32504*
[d] *Department of Analytical Chemistry, University of Granada, 18071 Granada, Spain*

by sensitivity to light and air, and interference from reducing agents.[26] Alternatively, LPMOs exhibit peroxidase-like activity, enabling spectrophotometric detection through H_2O_2-dependent oxidation of 2,6-dimethoxyphenol or hydrocoerulignone, forming coerulignone detectable at 469 nm.[27,28] A highly sensitive fluorometric assay has also been developed based on LPMO-catalysed oxidation of reduced fluorescein to fluorescein.[29] However, it is important to note that these assays, even though useful to study LPMO stability and functionality, do not provide direct information on the polysaccharide-dependent peroxygenase activity of LPMOs.

Discontinuous assays have also been established, including turbidity-based measurements of substrate depletion[30] and quantification of oxidised products by Ni^{2+} adsorption.[31] The Ni^{2+} adsorption assay measures C1-oxidation by detecting aldonic acid products through nickel ion binding.[31] Also, gluconic acid produced by C1-oxidising LPMOs can be quantified through the concomitant formation of NADPH, which is then measured spectrophotometrically.[32] However, these assays are limited to specific reaction conditions (turbidity assay), or require C1-oxidising LPMOs (Ni^{2+} assay, D-gluconic acid/D-glucono-δ-lactone assay kit). Additionally, a colourimetric assay using dyed azoxyloglucan detects activity through release of coloured oligosaccharides, though its general applicability is restricted to LPMOs active on xylan or its derived oligosaccharides.[24]

Alternatively, LPMO activity has also been measured *via* the determination of the depletion of the co-substrate H_2O_2. Accurate monitoring of enzyme activity *via* quantification of H_2O_2 is often complicated by its chemical instability and rapid reaction with reductants.[5,33] Recently, electrochemical methods have been applied to detect H_2O_2-depletion in LPMO reactions, thus providing real-time kinetic information.[17,34] A microsensor was used to detect the H_2O_2 consumption by fungal LPMOs acting on a native cellulose substrate (plant cell walls). The method provides high spatial resolution of H_2O_2 consumption but also requires a complex scanning electrochemical microscopy (SECM) platform.[17] Alternatively, consumption of H_2O_2 by LPMO on soluble and insoluble substrates was monitored in real-time using a gold rotating disc electrode modified with a thin layer of Prussian blue to achieve selective detection of H_2O_2.[34] This setup reduced diffusion limitations and allowed for a detailed insight into enzyme kinetics, stability, and substrate specificity of various tested LPMOs. While such electrochemical systems offer high selectivity due to the low applied potential (100 mV *vs.* SHE), they require expertise in electroanalytical techniques, specialised instrumentation and are challenging to implement for at-line monitoring of H_2O_2.

In this research, we employ an optical H_2O_2 sensor, first reported by Tjell *et al.*,[35,36] to monitor the activity of H_2O_2-generating and consuming enzymes. The sensor was previously applied to follow H_2O_2 formation by nitrogen-doped carbon nanodots[36] and to follow the enzymatically produced H_2O_2 by immobilised glucose oxidase in a model reactor.[35] We show that this sensor concept can be extended to the measurement of freely diffusing enzymes. Importantly, its low response time in the seconds range, its straightforward setup and the broad dynamic range from a few micromolar to a few hundred micromolar, make it a useful tool in biocatalysis for mechanistic studies as well as for process monitoring. Furthermore, the sensor exhibits minimal cross-sensitivities to interfering substances, with responses relative to H_2O_2 measured as 2.7% for sodium peroxynitrite, 0.2% for sodium hypochlorite, 0.1% for *tert*-butyl hydroperoxide, and 2.2% for ascorbic acid (each species tested at 100 μM). Salinity (10 mM phosphate buffer *vs.* filtered seawater) did not affect the sensor calibration.[35] We demonstrate its utility by following the activity of a H_2O_2-producing and a H_2O_2-consuming enzyme, glucose oxidase (GOD) and LPMO from *Lentinus similis* (*Ls*AA9A), respectively. *Ls*AA9A exhibits activity on both soluble oligosaccharides, as short as cellotriose, and insoluble polysaccharide substrates, including cellulose and xylan,[37–41] making it an ideal candidate for evaluating H_2O_2-driven oxidative activity. By directly tracking the consumption of H_2O_2 by the LPMO, which is utilised stoichiometrically with the formation of oxidised products (*e.g.*, one mole of H_2O_2 consumed per mole of oxidised sugar),[7] the sensor allows for a rapid, substrate-independent monitoring of the activity of this enzyme.

2 Results and discussion

2.1 Set-up of H_2O_2 optical sensor

The H_2O_2 sensor used was first reported by Tjell *et al.*[35] The setup used in these experiments (Fig. 1A and C) consists of luminescence-based sensing elements integrated into a flow cell. The sensing elements consist of a platinum-based catalyst and luminescent oxygen-sensitive particles embedded in a host polymer. The catalyst converts H_2O_2 in the sample solution into molecular oxygen (O_2), which is detected and quantified by the oxygen-sensitive particles. To eliminate the background from dissolved O_2 in the sample, the sample solution is pumped through sodium sulphite solution (Na_2SO_3, 2%) through a gas-permeable silicon tube to scavenge oxygen before entering the flow cell. Importantly, this avoids direct contact of the reaction mixture with Na_2SO_3.

The optical H_2O_2 sensor was evaluated using the H_2O_2-producing enzyme glucose oxidase in a homogeneous reaction system.

The optical H_2O_2 sensor enabled continuous, real-time measurement of H_2O_2 production in a concentration range of 5 μM to 200 μM.[35] To evaluate the suitability of the herein used setup for enzyme assays, glucose oxidase (GOD) was employed as a model H_2O_2-producing enzyme in a homogeneous aqueous environment. GOD catalyses the oxidation of glucose to gluconic acid, with the concurrent formation of H_2O_2. In measurements with the optical H_2O_2 sensor (Fig. 2A), we used a temporal resolution of 3 seconds, allowing for a *quasi*-continuous monitoring of the enzymatic reaction. In these experiments, we obtained a specific GOD activity of 5.1 U g_{enzyme}^{-1}, at pH 6 and 37 °C. To validate this

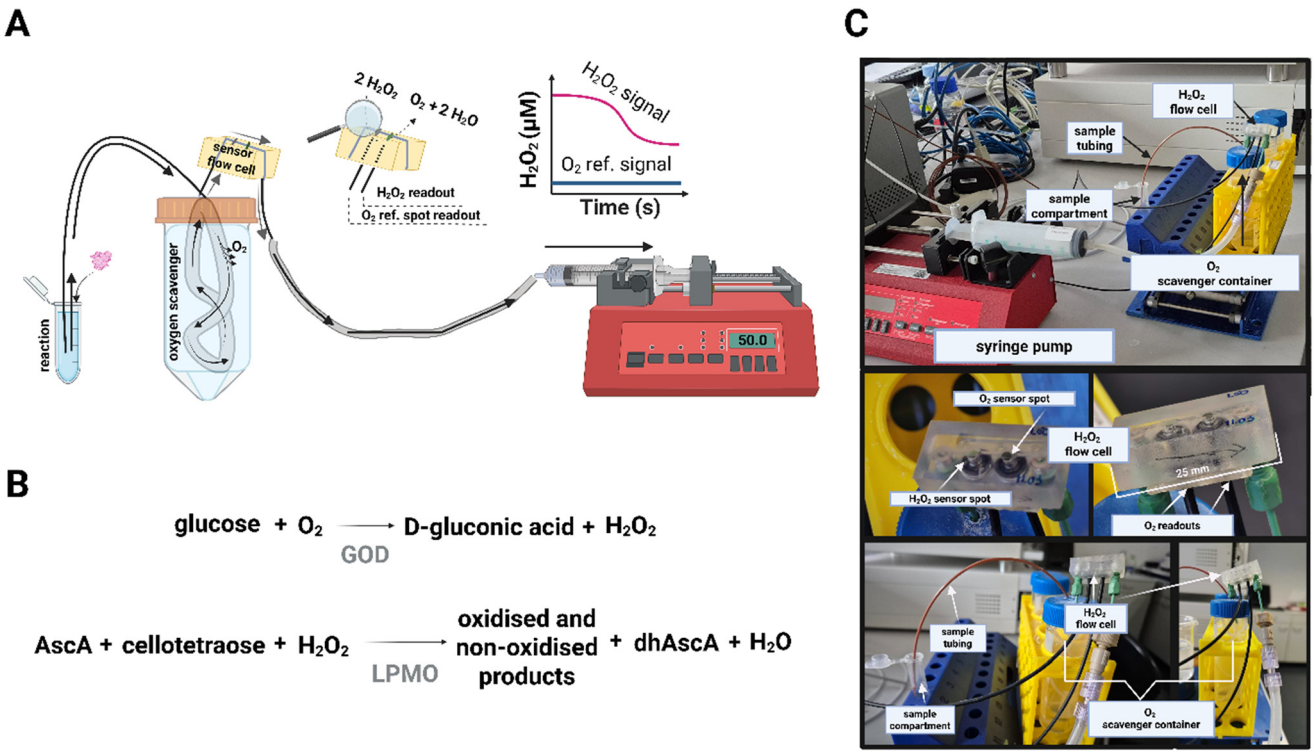

Fig. 1 Optical H_2O_2 sensor setup[35] and H_2O_2-dependent enzymatic reactions tested. (A) Schematic representation of the sensor setup. The reaction mixture passes through an oxygen scavenging solution of 2% Na_2SO_3 inside a gas-permeable but Na_2SO_3 impermeable silicone tube (l = 29 cm; OD = 2.5 mm) to scavenge atmospheric O_2 in the sample mixture. The flow cell (l = 25 mm) contains two sensor spots; one functions as an O_2 sensor, while the other includes the catalyst converting the H_2O_2 to O_2. The O_2 concentration is quantified through oxygen-sensitive particles. The H_2O_2 concentrations are calculated from the difference between both O_2 signals recorded on two separate channels. (Created with http://BioRender.com) (B) glucose oxidase (GOD) and *Ls*AA9A were used as H_2O_2-forming and H_2O_2-consuming enzymes, respectively, to test the optical sensor for monitoring of enzyme activity. GOD is an oxidase that oxidises glucose into D-glucono-1,5-lactone in the presence of O_2. The *Ls*AA9A cleaves both soluble and insoluble cello-oligosaccharides. Here we test the *Ls*AA9A with soluble cellotetraose in the presence of H_2O_2 and ascorbic acid as reducing agent for the reduction of the copper active centre of the enzyme (AscA = ascorbic acid; dhAscA = dehydroascorbic acid). http://BioRender.com (C) setup of the prototype optical H_2O_2 sensor in the laboratory. A syringe pump is used to pump the reaction mixture through the sensor system.

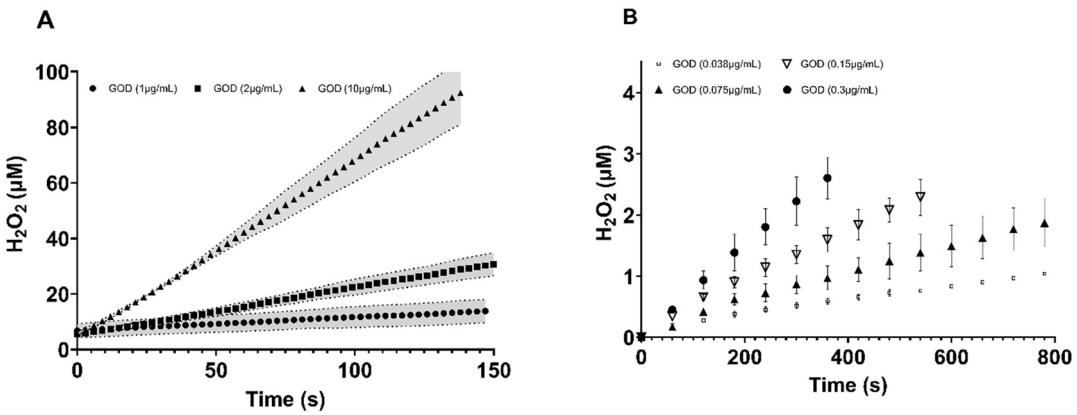

Fig. 2 Activity of glucose oxidase (GOD) with glucose measured with the H_2O_2 sensor (A) and by a spectrophotometric method using ABTS as chromogenic substrate (B). (A) The H_2O_2 produced by the oxidation of glucose by GOD is monitored by the H_2O_2 sensor. The grey area around the error bars indicates the standard deviation of duplicate reactions. (B) The amount of H_2O_2 produced by the oxidation of glucose by GOD is estimated by monitoring the absorbance increase given by the oxidation of the ABTS (ε_{420} = 36 mM^{-1} m^{-1}) at 570 nm. The amount of H_2O_2 formed during the reaction is equimolar to the amount of ABTS formed. Error bars are the standard deviations of the average of triplicates.

result, an orthogonal spectrophotometric method using 2,2′--azino-bis(3-ethylbenzothiazoline-6-sulfonic acid) (ABTS) as chromogenic substrate was employed using the same conditions. In this indirect method, ABTS is oxidised by

horseradish peroxidase in the presence of H_2O_2 produced by GOD, producing a measurable colour change (Fig. 2B). Through this method, we obtained a specific GOD activity of 7.9 U g_{enzyme}^{-1}. The discrepancy between the activity data, showing an approximately 1.5-times lower H_2O_2 formation rate of the optical sensor, can be explained by several factors. Notably, the photometric ABTS-coupled assay is limited to H_2O_2 concentrations below ~5 μM and requires sub-μM concentrations of GOD due to the strong absorbance of the formed ABTS cation radical. In contrast, the optical sensor can reliably detect H_2O_2 concentrations up to 80 μM (Fig. S2), allowing for a broader measurement range. The lower response of the H_2O_2 sensor may also result from the inherent delay associated with the design of the flow system. Before entering the optical flow cell, around 100 μL of reaction mixture passes through a deoxygenation module containing sodium sulphite, which is essential for minimising background interference caused by dissolved oxygen. This delay may result in partial degradation or disproportionation of the enzymatically produced H_2O_2, thus reducing the concentration of O_2 detected by the luminescence probe. Additionally, the internal catalytic activity of the flow cell and diffusion limitations might attenuate the sensor response further, especially during rapid enzymatic turnover. Despite this, these data demonstrate the general suitability of the sensor to measure enzyme reactions in which enzymes are freely diffusing.

2.2 Evaluation of optical H_2O_2 sensor using H_2O_2-degrading LPMO in homogeneous reaction systems

To assess H_2O_2 consumption, we selected an LPMO from *Lentinus similis* (*Ls*AA9A), a well-studied LPMO[38] exhibiting activity on both soluble oligosaccharides, as short as cellotriose, and insoluble polysaccharide substrates, including cellulose.[37–41] In this study, LPMO reactions were performed using 50 μM ascorbic acid (AscA) as the reducing agent together with cellotetraose, a soluble oligosaccharide substrate (Fig. 3A). Initial H_2O_2 concentrations were set at 50 μM, which falls within the range of commonly reported concentrations for LPMO activity determinations (50–100 μM). This is notable because many LPMOs are known to tolerate H_2O_2 concentrations only up to ~100 μM before the risk of autoxidative degradation becomes significant.[42] With the H_2O_2 sensor, the initially measured H_2O_2 concentrations showed deviations of 10–20% (Fig. 3A).

A series of control reactions were performed to distinguish background signals from enzymatic H_2O_2 consumption (Fig. 3A). Cellotetraose alone at a concentration of 0.1 mM did not interfere with the output signal, confirming the absence of the endogenous H_2O_2 and absence of interference caused by other contaminants present within the substrate solution. Reactions containing only ascorbic acid and H_2O_2, as well as those combining cellotetraose with H_2O_2 in the absence of enzyme, showed that none of the components individually or in combination interfered with the H_2O_2 detection. Additional controls included reactions containing only Cu(II), as well as enzyme preparations in which the copper cofactor had been chelated by EDTA (5000-fold molar excess over *Ls*AA9A) to assess the role of the active-site metal centre. These controls demonstrated that H_2O_2 consumption only occurs in the copper-bound state of the enzyme and in the presence of all reaction components (Fig. 3A).

Additional reactions were conducted with or without ascorbic acid and cellotetraose. Control reactions containing *Ls*AA9A and H_2O_2 in the absence of cellotetraose showed a slow decrease in the H_2O_2 concentration, possibly due to the release of copper upon enzyme deactivation.[42] However, these reactions were at least an order of magnitude slower than the substrate-dependent turnover and not significant within the observed timeframe (data not shown).

Assays containing all reaction components were initiated by the addition of *Ls*AA9A at varying concentrations (Fig. 3A and B). The enzyme was added after the stabilisation of the H_2O_2 signal. After a short lag phase, a decrease in H_2O_2 was observed, indicative of LPMO catalysis (Fig. 3A and B). Reaction rates were calculated from the initial slopes of the reactions shown in Fig. 3B. Notably, the rates of H_2O_2-depletion were proportional to the employed *Ls*AA9A concentration (Fig. 3B and C). Additionally, samples were periodically withdrawn during the assay and oxidised products were quantified.[32] The time-dependent formation of oxidised products corroborated the activity of the *Ls*AA9A on the tetraose substrate (Fig. S3). Of note, H_2O_2 was not fully consumed during the reactions, which levelled off after approximately 90–120 seconds. This is indicative of (partial) enzyme deactivation, likely due to incomplete active-site saturation. This suggests that soluble cello-oligosaccharides are not suitable for sustained LPMO turnover (see below, section 2.4).

The activity towards cellotetraose was further tested by applying the *Ls*AA9A in the fast colourimetric assay using 2,6-DMP as a chromogenic reagent. This assay is based on the peroxidase side-reactivity of LPMOs, in which 2,6-DMP is oxidised to coerulignone in the presence of H_2O_2.[27,28] This assay does not measure the substrate-dependent turnover of LPMOs; however, when carried out in the presence of the substrate cellotetraose, the DMP assay was effectively suppressed, indicating the interaction of the *Ls*AA9A with cellotetraose[41] (see Fig. S4). A similar effect was previously observed for the oxygen-reducing side reactivity of *Nc*LPMO9C, an LPMO from *Neurospora crassa*, for cello-oligosaccharides with a higher degree of polymerisation.[10]

2.3 Post-reaction H_2O_2 accumulation indicates LPMO inactivation *via* self-oxidation

Fig. 4 presents the concentration of H_2O_2 measured over time following the completion of biocatalytic reactions using *Ls*AA9A with varying concentrations of cellotetraose as substrate. A slow, but notable post-reaction accumulation of H_2O_2 levels was observed, suggesting that the enzyme

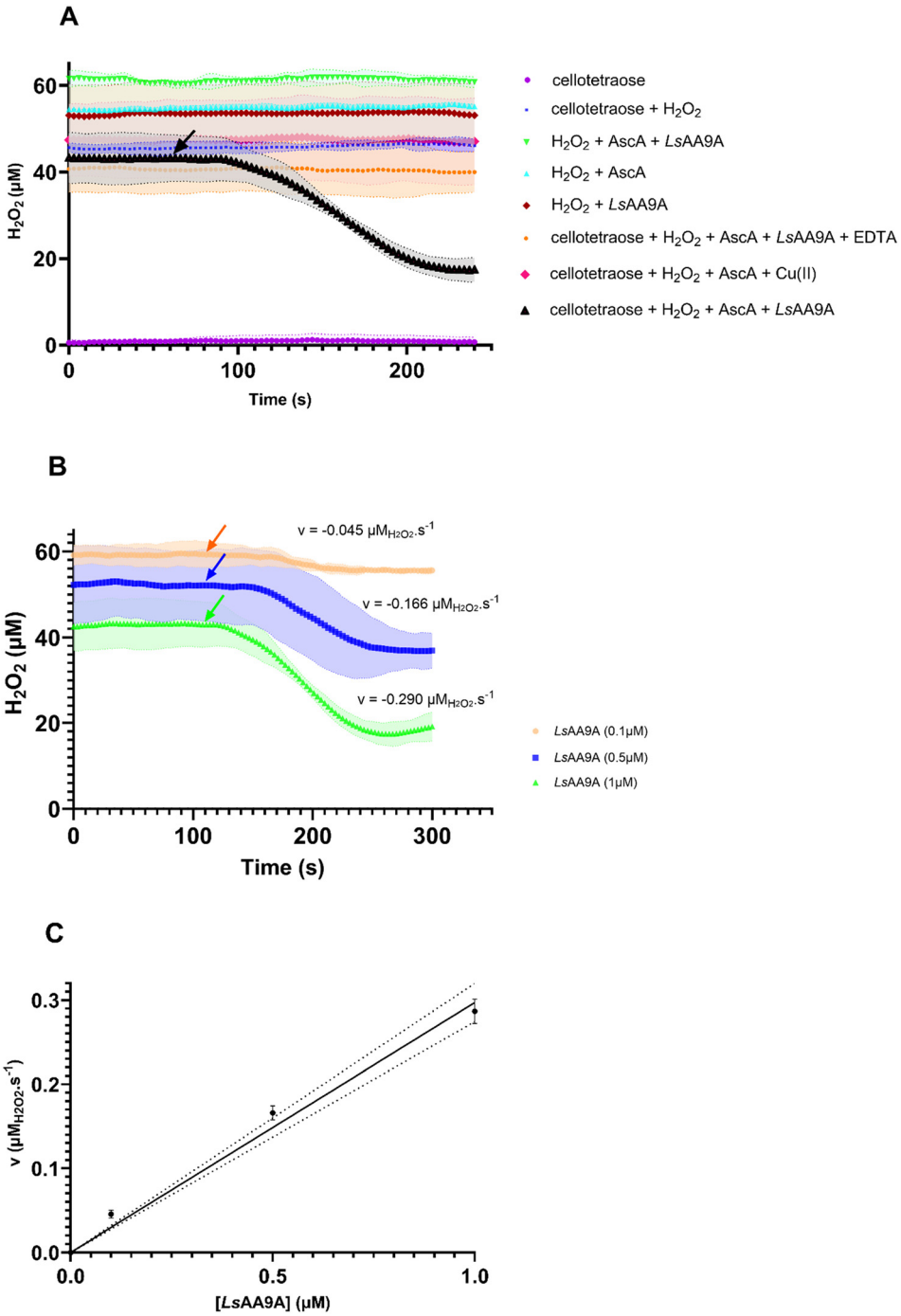

Fig. 3 Monitoring of the activity of *Ls*AA9A with soluble cellotetraose using the H_2O_2 sensor. (A) Control reactions: cellotetraose (0.05–1 mM); cellotetraose (0.1 mM) + H_2O_2 (50 μM); H_2O_2 (50 μM) + AscA (50 μM) + *Ls*AA9A (1 μM); H_2O_2 (50 μM) + AscA (50 μM); H_2O_2 (50 μM) + *Ls*AA9A (1 μM); cellotetraose (0.1 mM) + H_2O_2 (50 μM) + AscA (50 μM) + *Ls*AA9A (1 μM) + EDTA (5 mM); cellotetraose (0.1 mM) + H_2O_2 (50 μM) + AscA (50 μM) + $CuCl_2$ (0.65 μM); and complete LPMO reaction with cellotetraose: cellotetraose (0.1 mM) + H_2O_2 (50 μM) + AscA (50 μM) + *Ls*AA9A (1 μM). Reactions were performed in 1 mL total volume, and *Ls*AA9A was added after stabilisation of the H_2O_2 signal. The addition of *Ls*AA9A is indicated by a black arrow. Data points reflect the average of two independent replicates, with the coloured region denoting the error range of both replicates. (B) *Ls*AA9A reaction with cellotetraose using different enzyme concentrations (0.1 μM; 0.5 μM; 1 μM). The start of reactions is shown by arrows. Data points reflect the average of two independent replicates, with the coloured region denoting the error range of both replicates. (C) Velocity of reaction given by initial slopes of H_2O_2 degradation *versus* concentration of *Ls*AA9A.

undergoes inactivation.[7,42–44] This is attributed to two primary pathways: (i) the reaction of reduced LPMO with molecular oxygen (O_2), leading to the formation of H_2O_2, and (ii) a direct reaction of the reduced LPMO with H_2O_2 itself, a self-oxidative process that occurs in the absence of substrate.[41] These pathways have been well-characterised for

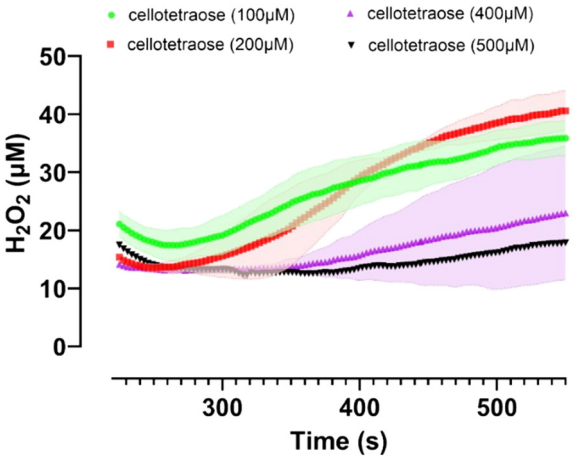

Fig. 4 Post-reaction H_2O_2 accumulation following LPMO activity on cellotetraose. After completion of the LPMO reaction – marked by the cessation of H_2O_2 consumption – a subsequent increase in H_2O_2 concentration indicates continued H_2O_2 production by the *Ls*AA9A. This suggests LPMO inactivation through self-oxidation. At higher cellotetraose concentrations, this post-reaction H_2O_2 accumulation is delayed, likely due to slower desorption of the LPMO from the oxidised substrate, thereby postponing the onset of self-oxidation compared to reactions with lower cellotetraose concentrations.

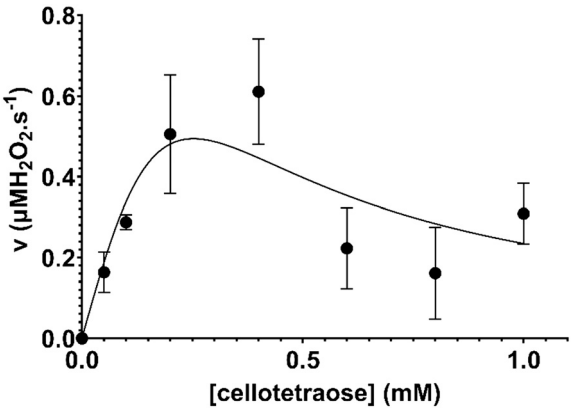

Fig. 5 Michaelis–Menten kinetics of *Ls*AA9A with soluble cellotetraose. The velocities were estimated through the initial slopes of the reactions in the linear range for each cellotetraose concentration (0.05–1 mM). Substrate inhibition is present. Error bars are standard deviations of the average values of duplicates.

LPMOs acting on insoluble polysaccharides,[41] where prolonged desorption from the substrate surface increases the risk of inactivation. Here, we show the same phenomenon for soluble cellotetraose. It should be noted that cello-oligosaccharides are probably not the preferred substrates, indicated by the high Michaelis–Menten constant (K_M) of *Ls*AA9A for cellotetraose of 0.22 mM (see section 2.4). Notably, the rates of H_2O_2 accumulation in these experiments inversely correlated with the initial substrate concentration. At higher cellotetraose concentrations, the enzyme appears to remain bound to the substrate for longer periods, thereby delaying desorption and the onset of inactivation. This extended substrate interaction offers a protective effect, reducing the frequency of uncoupled turnovers that generate damaging reactive oxygen species. These findings indicate that substrate availability plays a crucial role in modulating LPMO lifetime and activity. The self-inactivation of the enzyme after the reaction with cellotetraose was confirmed by determination of the post-reaction residual activity using the colourimetric 2,6-DMP assay (see Fig. S5). After the reaction, the *Ls*AA9A retained only 11% of its initial activity, indicating substantial oxidative damage.

2.4 *Ls*AA9A kinetics with cellotetraose

To further understand the catalytic performance of *Ls*AA9A, kinetic parameters were determined (Fig. 5) using the optical H_2O_2 sensor. Steady-state kinetics yielded a Michaelis–Menten constant (K_M) of 0.22 ± 0.08 mM and a maximum reaction rate (V_{max}) of 0.97 ± 0.64 μM s^{-1} (see Fig. S6 and S7). The *Ls*AA9A showed substrate inhibition, with an apparent K_i of 212 nM, an effect that had already been previously observed for this enzyme and substrate.[41] Specifically, the cleavage of fluorescently labelled cellotetraose revealed a K_M of 43 ± 9 μM and a catalytic turnover rate (k_{cat}) of 0.11 ± 0.01 s^{-1} at pH 7.0 and 37 °C, with reaction kinetics fitting well to classic Michaelis–Menten behaviour.[45] However, these constants were obtained under different reaction conditions and, notably, in the absence of H_2O_2, making a direct comparison difficult. The obtained K_M value of 43 ± 9 μM is low, compared to the one obtained in our study (0.22 mM). The difference could be partly due to the presence of aromatic groups at the reducing and non-reducing ends of the fluorescently labelled substrate cellotetraose.[45] In support, the K_M for another similar cello-oligosaccharide, cellopentaose, obtained for another known LPMO, *Nc*AA9C, in the presence of H_2O_2, was also significantly higher (2.1 ± 0.3 mM, at 4 °C).[16]

3 Conclusions

In this study, an optical H_2O_2 sensor was validated for both H_2O_2-producing and -consuming redox enzymes in a homogenous reaction setup. Using glucose oxidase as a model enzyme, we show that the sensor enables reliable real-time detection of H_2O_2 formation, matching activity measurements obtained by spectrophotometric methods. More importantly, this study introduces a versatile and sensitive approach for monitoring LPMO activity based on H_2O_2 turnover. Importantly, these measurements are independent of the oxidation mode of the enzyme (C1, C4 or mixed oxidation) and can potentially be used with a variety of different substrates and with different reaction conditions. Despite the advantages, some limitations remain in the current implementation. Notably, there is a need to optimise the deoxygenation step preceding H_2O_2 detection. The currently required lag time between sample injection and flow cell detection introduces a delay that may affect the accurate timing of signal onset. While this does not affect

steady-state comparisons, it may hinder the resolution of rapid kinetic events, especially in reactions with fast initial rates or short-lived intermediates. Overall, the optical sensor extends the portfolio of currently available methods for the determination of LPMO reactions and enables broader application for other peroxidases and peroxygenases.

4 Experimental

4.1 Materials and reagents

Glucose oxidase from *Aspergillus niger* (type VII, lyophilized powder) was purchased from Merck. Cellotetraose (purity > 90%) was purchased from Megazyme. β-Glucosidase (10–50 units per mg) was purchased from Merck. D-Gluconic acid/D-glucono-*δ*-lactone assay kit was purchased from Megazyme.

4.2 Production of *Ls*AA9A

Production of *Ls*AA9A from *Lentinus similis* was carried out as described previously.[46] *Ls*AA9A (EC 1.14.99.56, GenBank ALN96977.1), with a C-terminal double strep tag II, was ordered in the pET28a expression vector (ATG Biosynthetics, Germany) (Fig. S1). Chemically competent *E. coli* BL21 cells were transformed with the pET28a *Ls*AA9A vector and plated onto LB agar containing 40 μg mL^{-1} kanamycin. A single colony was introduced into 4 mL LB medium (containing 40 μg mL^{-1} kanamycin) and cultured for 18 h. The culture was used to inoculate 400 mL of 2xYT auto induction medium supplemented with 100 μg mL^{-1} kanamycin and grown for 3.5 h at 37 °C, followed by a further incubation at 25 °C for 39 h (130 rpm). The cells were harvested by centrifugation (6000 rpm, 4 °C, 30 min) and stored at −20 °C until further use.

The frozen cell pellets were thawed on ice for 1 h and resuspended in cold NP buffer (50 mM NaH_2PO_4, pH 8; 300 mM NaCl). The mixture was sonicated for 2 × 5 min at 50% power (Branson Sonifier, Sigma-Aldrich) and cell debris was removed by centrifugation (12 000 rpm, 4 °C, 1 h). The supernatant was filtered through a 0.2 μm syringe filter and loaded onto a 5 mL Strep-Tactin®X column (Cytiva) using an ÄKTA Pure chromatographic system (GE Healthcare). The column was washed with NP buffer to remove the unbound proteins. Finally, the apo-*Ls*AA9A was eluted at once with NPB buffer (50 mM NaH_2PO_4, pH 8; 300 mM NaCl, 50 mM biotin). The enzyme solution was concentrated and rebuffered to potassium phosphate (50 mM, pH 6.0) using Vivaspin 20 centrifugal concentrators with a 10 kDa molecular weight cut-off. The protein concentration was determined by the Bradford method using bovine serum albumin for calibration.

To generate copper-loaded *Ls*AA9A, $CuCl_2$ (10 mM in Milli-Q water) was slowly added to the apo-protein in a ratio apo-protein : copper of 1.5 : 1, followed by incubation on ice for 2 h without any further desalting and concentration steps (from 6 × 300 mL cultures, approximately 18 mg of *Ls*AA9A were produced).

4.3 Glucose oxidase activity assay

The activity of the commercial glucose oxidase was assessed as described previously.[30] In summary, the H_2O_2-dependent oxidation of the chromogenic reagent 2,2′-azino-bis(3-ethylbenzothiazoline-6-sulfonic acid) (ABTS) by horseradish peroxidase (HRP) was measured spectrophotometrically, which depends on the formation of H_2O_2 by the glucose oxidase (GOD) (eqn (1) and (2)). The oxidation of ABTS (ε_{420} = 36 mM^{-1} cm^{-1}) was continuously monitored by following the increase in absorbance at 420 nm.

GOD activity was assayed with 10 mM glucose in 50 mM phosphate buffer, pH 6, using 7 U ml^{-1} HRP and 1 mM ABTS as chromogenic substrate. Reactions had a final volume of 200 μL and were measured in the 96-well plate format using a plate reader (BioTek Synergy, Agilent). Absorbance was continuously read at 570 nm for 25 min at 37 °C. One unit of enzyme activity was defined as the amount of GOD that oxidised 1 μmol of ABTS per minute under the specified assay conditions.

$$\text{D-glucose} + H_2O + O_2 \xrightarrow[\text{GOD}]{} \text{Gluconic acid} + H_2O_2 \quad (1)$$

$$H_2O_2 + \text{ABTS(red)} \xrightarrow[\text{HRP}]{} H_2O + \text{ABTS(ox)} \quad (2)$$

4.4 Preparation of the H_2O_2 sensor

The H_2O_2 sensor used was first reported by Tjell *et al.*[35] The setup used in these experiments (Fig. 1A and C) consists of luminescence-based sensing elements integrated into a flow cell. The sensing element contains a platinum-based catalyst and luminescent oxygen sensitive particles embedded in a host polymer. The catalyst converts H_2O_2 in the sample solution into molecular oxygen (O_2), which is detected and quantified by the oxygen sensitive particles. To eliminate the background from dissolved O_2 in the sample, the sample solution is pumped through sodium sulphite solution (Na_2SO_3, 2%), using a gas-permeable tube, to scavenge oxygen before entering the flow cell.

The optical sensors were prepared from liquid sensor formulations as described previously.[35] In brief, for O_2 sensors, 2% palladium(II)-6,13,20,27-tetrakis(4-fluorophenyl) tetrabenzoporphyrin (PdTPTBPF) immobilized on PS/DVB beads dispersed in 7% Hydromed™ D7 in 9 : 1 EtOH/H_2O were used. H_2O_2 sensors were prepared by adding 60 mg mL^{-1} of nanosilica-supported platinum nanoparticles (PtNP) to the O_2 sensor formulation. The formulations were coated on a polyethylene glycol terephthalate (PET) support and glued into the flow-through. The cell was closed with pressure-sensitive adhesive tape (ThermalSeal RTS™, Excel Scientific, Inc., USA). The total internal volume of the sensor system (sample tube + deoxygenation tube + flow cell tube) was approx. 135 μL.

For sensor read-outs a fibre-optic oxygen meter was used (FireSting, Pyroscience GmbH, Germany). A temperature sensor was placed in proximity to the flow cell to allow temperature-dependent O_2 measurements. All data was

recorded with the Pyro Oxygen Logger software (PyroScience GmbH, Germany) using two channels: channel 1 records the O_2 formation by the platinum catalyst, while channel 2 records the baseline O_2 level, which typically is below 2 mbar after deoxygenation. Channel 3 records the temperature.

The sensor was used for monitoring the activity of H_2O_2-generating and H_2O_2-consuming enzymes in solution. In all experiments, a sample flow of 50 μL min^{-1} was maintained using a syringe pump (New Era Instruments). Before each run, an extensive deoxygenation step was performed either overnight or for at least 8 hours by pumping degassed MQH_2O through the sensor setup. The temperature was also recorded, and data points were logged every 3 seconds. Calibrations were performed with MQH_2O and fresh stock solutions prepared by diluting 30% H_2O_2. Values of the calibration curve are averaged from continuous three-minute measurements (Fig. S2).

4.5 H_2O_2 sensor experiments for enzyme activity monitoring

GOD was assayed using the H_2O_2 sensor with 10 mM glucose in 50 mM phosphate buffer, pH 6, at 37 °C ± 1 °C. The reaction was performed using 2 mL conical tubes (Eppendorf, Germany). Reactions (excluding GOD) were prepared in a final volume of 1 mL, and the enzyme was added only after stabilisation of the H_2O_2 signal after approx. 10 min. All reactions were performed in a volume of 500 μL. The temperature was recorded, and data points were logged every 3 seconds. From the data points obtained by the sensor, concentrations of H_2O_2 were determined according to the calibration curve (Fig. S2).

*Ls*AA9A, as a H_2O_2-consuming enzyme, was measured with the same sensor setup. Ascorbic acid (AscA) was used as a reductant, and cellotetraose was supplied as substrate. One μM *Ls*AA9A was assayed with soluble cellotetraose (0.05–1 mM), 50 μM H_2O_2 and 50 μM AscA in 50 mM phosphate buffer, pH 6, at 20 °C ± 1 °C. The reactions were performed in 2 mL conical tubes (Eppendorf). Reactions (excluding *Ls*AA9A) were prepared in a final volume of 2 mL, and the enzyme was added only after stabilisation of the H_2O_2 signal after 20 min. The final reaction was performed in 1 mL volume. Control reactions that contained only cellotetraose at varying concentrations (0.1–1 mM), AscA (50 μM) in combination with H_2O_2 (50 μM), or cellotetraose (0.1 mM) in combination with H_2O_2 (50 μM) were performed to monitor the occurrence of non-enzymatic side reactions. *Ls*AA9A was also studied in the absence and presence of cellotetraose. Additionally, the H_2O_2-consuming reaction by the selected LPMO was performed with and without reductant. A control using only Cu(II) was also performed as well as a reaction where the copper-dependent enzyme was chelated by EDTA 5 mM. The temperature was recorded, and data points were logged every 3 seconds. From the data points, given by the sensor, concentrations of H_2O_2 were determined according to the calibration curve (Fig. S2).

4.6 Activity of *Ls*AA9A using a colorimetric assay

The H_2O_2-dependent activity of *Ls*AA9A was assessed using 2,6-dimethoxyphenol (2,6-DMP) as described previously.[27,28] The activity was measured before and after the reaction with cellotetraose (0.1 mM) and also in the presence and absence of cellotetraose (0.1–0.5 mM). Specifically, assays contained 10 mM 2,6-DMP, 50 μM H_2O_2 in 50 mM phosphate buffer, pH 6, and 4 μM of *Ls*AA9A were used. Reactions had a total volume of 200 μL and were followed at 469 nm in a 96-well plate using a plate reader (BioTek Synergy, Agilent). One unit of LPMO activity was defined as the amount of LPMO that oxidises 2 μmol 2,6-DMP to 1 μmol coerulignone (ε_{469} = 53 200 M^{-1} cm^{-1}) per min under the specified reaction conditions.

4.7 Quantification of product formation by *Ls*AA9A

The reaction with *Ls*AA9A was performed by adding 1 μM *Ls*AA9A to cellotetraose (0.1 mM), 50 μM H_2O_2 and 50 μM AscA in 50 mM phosphate buffer, pH 6, at 20 °C ± 1 °C. The reactions were performed using 2 mL conical tubes (Eppendorf) at a volume of 1 mL. 100 μL of the reaction mixture was sampled before the addition of the enzyme and after 20 s and 120 s. The collected samples were incubated with β-glucosidase at 50 °C overnight to release glucose and gluconic acid/gluconolactone from the LPMO reaction products. The resulting gluconic acid was quantified using the D-gluconic acid/D-glucono-δ-lactone assay kit from Megazyme. This assay detects gluconic acid or D-glucono-lactone by reacting it with gluconate kinase and gluconate-6-phosphate dehydrogenase, with the concomitant formation of NADPH that can be followed spectrophotometrically at 340 nm.

4.8 Data processing

GraphPad Prism (10.4.1, Dotmatics) was used to generate graphics and modelling of the kinetics of *Ls*AA9A. Activities were calculated from initial slopes of the reactions.

Author contributions

D. K. and T. M. conceived the study. L. V. C. assisted in designing the experiments and conducted the experimental work. A. T. developed the prototype H_2O_2 optical sensor and established its setup, providing all materials. A. Ø. T. and T. M. contributed to the verification of H_2O_2 sensor and interpretation of the signal. L. V. C and D. K. were responsible for data interpretation and curation. M. D. F. R. supported the initial calibrations. L. V. C. and D. K. wrote the first draft of the manuscript. All authors contributed to the writing, review, and editing of the manuscript and approved the final version.

Conflicts of interest

All authors declare that they have no conflicts of interest and no competing financial interests.

Data availability

All kinetic measurements generated and analyzed during this study are fully presented in the main manuscript. Supporting data, including SDS-PAGE analyses confirming enzyme purity, calibration curves, and DNA sequences of the investigated enzymes, are provided in the supplementary information (SI) uploaded with the manuscript.

Supplementary information is available. See DOI: https://doi.org/10.1039/d5re00332f.

Acknowledgements

This work was supported by the BioTechMed-Graz Young Researcher Group Program (D.K., L.V.C.). M.D.F.R. is grateful to the Ministry of Science, Innovation and Universities of Spain for a mobility grant "Salvador de Madariaga" (PRX22/00487).

References

1 D. Monti, G. Ottolina, G. Carrea and S. Riva, *Chem. Rev.*, 2011, **111**, 4111–4140.
2 A. J. C. Wahart, J. Staniland, G. J. Miller and S. C. Cosgrove, *R. Soc. Open Sci.*, 2021, **8**, 211572, DOI: 10.1098/rsos.211572.
3 M. Hobisch, D. Holtmann, P. Gomez de Santos, M. Alcalde, F. Hollmann and S. Kara, *Biotechnol. Adv.*, 2021, **51**, 107615.
4 B. Bissaro, A. Várnai, Å. K. Røhr and V. G. H. Eijsink, *Microbiol. Mol. Biol. Rev.*, 2018, **82**(4), DOI: 10.1128/MMBR.00029-18.
5 B. O. Burek, S. Bormann, F. Hollmann, J. Z. Bloh and D. Holtmann, *Green Chem.*, 2019, **21**, 3232–3249.
6 G. Vaaje-Kolstad, B. Westereng, S. J. Horn, Z. Liu, H. Zhai, M. Sørlie and V. G. H. Eijsink, *Science*, 2010, **330**, 219–222.
7 B. Bissaro, Å. K. Røhr, G. Müller, P. Chylenski, M. Skaugen, Z. Forsberg, S. J. Horn, G. Vaaje-Kolstad and V. G. H. Eijsink, *Nat. Chem. Biol.*, 2017, **13**(10), 1123–1128.
8 R. J. Quinlan, M. D. Sweeney, L. Lo Leggio, H. Otten, J.-C. N. Poulsen, K. S. Johansen, K. B. R. M. Krogh, C. I. Jørgensen, M. Tovborg, A. Anthonsen, T. Tryfona, C. P. Walter, P. Dupree, F. Xu, G. J. Davies and P. H. Walton, *Proc. Natl. Acad. Sci. U. S. A.*, 2011, **108**, 15079–15084.
9 C. M. Phillips, W. T. Beeson, J. H. Cate and M. A. Marletta, *ACS Chem. Biol.*, 2011, **6**, 1399–1406.
10 T. Isaksen, B. Westereng, F. L. Aachmann, J. W. Agger, D. Kracher, R. Kittl, R. Ludwig, D. Haltrich, V. G. H. Eijsink and S. J. Horn, *J. Biol. Chem.*, 2014, **289**, 2632–2642.
11 K. S. Johansen, *Biochem. Soc. Trans.*, 2016, **44**, 143–149.
12 T. M. Vandhana, J.-L. Reyre, D. Sushmaa, J.-G. Berrin, B. Bissaro and J. Madhuprakash, *New Phytol.*, 2022, **233**, 2380–2396.
13 A. Munzone, V. G. H. Eijsink, J.-G. Berrin and B. Bissaro, *Nat. Rev. Chem.*, 2024, **8**, 106–119.
14 D. Kracher, T. Lanzmaier and L. V. Carneiro, *Biochim. Biophys. Acta, Proteins Proteomics*, 2024, **1872**, 141012.
15 S. M. Jones, W. J. Transue, K. K. Meier, B. Kelemen and E. I. Solomon, *Proc. Natl. Acad. Sci. U. S. A.*, 2020, **117**, 11916–11922.
16 L. Rieder, A. A. Stepnov, M. Sørlie and V. G. H. Eijsink, *Biochemistry*, 2021, **60**, 3633–3643.
17 H. Chang, N. Gacias Amengual, A. Botz, L. Schwaiger, D. Kracher, S. Scheiblbrandner, F. Csarman and R. Ludwig, *Nat. Commun.*, 2022, **13**, 1–11.
18 R. Kont, B. Bissaro, V. G. H. Eijsink and P. Väljamäe, *Nat. Commun.*, 2020, **11**, 5786.
19 I. A. Christensen, V. G. H. Eijsink, A. A. Stepnov, G. Courtade and F. L. Aachmann, *Biochemistry*, 2023, **62**, 1976–1993.
20 F. Filandr, D. Kavan, D. Kracher, C. V. F. P. Laurent, R. Ludwig, P. Man and P. Halada, *Biomolecules*, 2020, **10**, 242.
21 A. Paradisi, E. M. Johnston, M. Tovborg, C. R. Nicoll, L. Ciano, A. Dowle, J. McMaster, Y. Hancock, G. J. Davies and P. H. Walton, *J. Am. Chem. Soc.*, 2019, **141**, 18585–18599.
22 G. R. Hemsworth, *Essays Biochem.*, 2023, **67**, 585–595.
23 B. Westereng, J. S. M. Loose, G. Vaaje-Kolstad, F. L. Aachmann, M. Sørlie and V. G. H. Eijsink, *Methods Mol. Biol.*, 2018, **1796**, 219–246.
24 F. Calderaro, L. E. Bevers and M. A. van den Berg, *Biomolecules*, 2021, **11**, 1098.
25 L. Schwaiger, A. Zenone, F. Csarman and R. Ludwig, *Methods Enzymol.*, 2023, **679**, 381–404.
26 A. A. Stepnov and V. G. H. Eijsink, *Methods Enzymol.*, 2023, **679**, 163–189.
27 E. Breslmayr, M. Hanžek, A. Hanrahan, C. Leitner, R. Kittl, B. Šantek, C. Oostenbrink and R. Ludwig, *Biotechnol. Biofuels*, 2018, **11**, 1–13.
28 E. Breslmayr, S. Daly, A. Požgajčić, H. Chang, T. Rezić, C. Oostenbrink and R. Ludwig, *Biotechnol. Biofuels*, 2019, **12**(283), DOI: 10.1186/S13068-019-1624-3.
29 J. Ipsen, K. S. Johansen and S. Brander, *Front. Microbiol.*, 2023, **14**, 1128470.
30 F. Filandr, P. Man, P. Halada, H. Chang, R. Ludwig and D. Kracher, *Biotechnol. Biofuels*, 2020, **13**, 1–13.
31 D. Wang, J. Li, A. C. Y. Wong, F. L. Aachmann and Y. S. Y. Hsieh, *Biotechnol. Biofuels*, 2018, **11**, 1–11.
32 M. B. Keller, C. Felby, C. A. Labate, V. O. A. Pellegrini, P. Higasi, R. K. Singh, I. Polikarpov and B. M. Blossom, *Biotechnol. Lett.*, 2020, **42**, 93–102.
33 J. Shen, P. T. Griffiths, S. J. Campbell, B. Utinger, M. Kalberer and S. E. Paulson, *Sci. Rep.*, 2021, **11**, 1–14.
34 L. Schwaiger, F. Csarman, H. Chang, O. Golten, V. G. H. Eijsink and R. Ludwig, *ACS Catal.*, 2024, **14**, 1205–1219.
35 A. Tjell, B. Jud, R. Schaller-Ammann and T. Mayr, *Sens. Actuators, B*, 2024, **400**, 134904.
36 A. I. Tjell, L. E. Meyer, B. Jud, S. Kara and T. Mayr, *React. Chem. Eng.*, 2024, **9**, 777–781.
37 R. Tokin, K. E. H. Frandsen, J. Ø. Ipsen, L. Lo Leggio, M. M. Poojary, J. G. Berrin, S. Grisel, S. Brander, P. E. Jensen and K. S. Johansen, *New Phytol.*, 2021, **232**, 1337–1349.
38 T. Tandrup, T. Tryfona, K. E. H. Frandsen, K. S. Johansen, P. Dupree and L. Lo Leggio, *Biochemistry*, 2020, **59**, 3347–3358.
39 T. Tandrup, L. Lo Leggio, F. Meilleur and M. J. Romao, *Acta Crystallogr., Sect. F: Struct. Biol. Commun.*, 2023, **79**, 1–7.

40 M. Frommhagen, A. H. Westphal, W. J. H. van Berkel and M. A. Kabel, *Front. Microbiol.*, 2018, **9**, 358610.
41 S. Brander, R. Tokin, J. Ipsen, P. E. Jensen, C. Hernández-Rollán, M. H. H. Nørholm, L. Lo Leggio, P. Dupree and K. S. Johansen, *ACS Catal.*, 2021, **11**, 13848–13859.
42 S. Kuusk, V. G. H. Eijsink and P. Väljamäe, *J. Biol. Chem.*, 2023, **299**, 105094.
43 G. Müller, P. Chylenski, B. Bissaro, V. G. H. Eijsink and S. J. Horn, *Biotechnol. Biofuels*, 2018, **11**, 1–17.
44 D. Kracher, M. Andlar, P. G. Furtmüller and R. Ludwig, *J. Biol. Chem.*, 2017, **293**, 1676.
45 K. E. H. Frandsen, T. J. Simmons, P. Dupree, J. C. N. Poulsen, G. R. Hemsworth, L. Ciano, E. M. Johnston, M. Tovborg, K. S. Johansen, P. Von Freiesleben, L. Marmuse, S. Fort, S. Cottaz, H. Driguez, B. Henrissat, N. Lenfant, F. Tuna, A. Baldansuren, G. J. Davies, L. Lo Leggio and P. H. Walton, *Nat. Chem. Biol.*, 2016, **12**(4), 298–303.
46 J. Zhao, Y. Zhuo, D. E. Diaz, M. Shanmugam, A. J. Telfer, P. J. Lindley, D. Kracher, T. Hayashi, L. S. Seibt, F. J. Hardy, O. Manners, T. M. Hedison, K. A. Hollywood, R. Spiess, K. M. Cain, S. Diaz-Moreno, N. S. Scrutton, M. Tovborg, P. H. Walton, D. J. Heyes and A. P. Green, *J. Am. Chem. Soc.*, 2023, **145**, 20672–20682.